Giovambattista Capasso, Maria Rizzo, Maria Lisa Garavaglia, Francesco Trepiccione, Miriam Zacchia, Alessandra Mugione, Patrizia Ferrari, Markus Paulmichl, Florian Lang, Johannes Loffing, Monique Carrel, Sara Damiano, Carsten A. Wagner, Giuseppe Bianchi and Giuliano Meyer
Am J Physiol Renal Physiol 295:556-567, 2008. First published May 14, 2008;
doi:10.1152/ajprenal.00340.2007

You might find this additional information useful...

This article cites 46 articles, 27 of which you can access free at:
http://ajprenal.physiology.org/cgi/content/full/295/2/F556#BIBL

Updated information and services including high-resolution figures, can be found at:
http://ajprenal.physiology.org/cgi/content/full/295/2/F556

Additional material and information about ***AJP - Renal Physiology*** can be found at:
http://www.the-aps.org/publications/ajprenal

This information is current as of April 27, 2009 .

AJP - Renal Physiology publishes original manuscripts on a broad range of subjects relating to the kidney, urinary tract, and their respective cells and vasculature, as well as to the control of body fluid volume and composition. It is published 12 times a year (monthly) by the American Physiological Society, 9650 Rockville Pike, Bethesda MD 20814-3991. Copyright © 2005 by the American Physiological Society. ISSN: 0363-6127, ESSN: 1522-1466. Visit our website at http://www.the-aps.org/.

Downloaded from ajprenal.physiology.org on April 27, 2009

Am J Physiol Renal Physiol 295: F556–F567, 2008.
First published May 14, 2008; doi:10.1152/ajprenal.00340.2007.

Upregulation of apical sodium-chloride cotransporter and basolateral chloride channels is responsible for the maintenance of salt-sensitive hypertension

Giovambattista Capasso,[1] Maria Rizzo,[1] Maria Lisa Garavaglia,[7] Francesco Trepiccione,[1] Miriam Zacchia,[1] Alessandra Mugione,[1] Patrizia Ferrari,[2] Markus Paulmichl,[6] Florian Lang,[3] Johannes Loffing,[4] Monique Carrel,[4] Sara Damiano,[1] Carsten A. Wagner,[4] Giuseppe Bianchi,[5] and Giuliano Meyer[7]

[1]*Department of Internal Medicine, Chair of Nephrology, Faculty of Medicine, Second University of Napoli, Napoli, Italy;* [2]*Prassis Research Institute, Sigma Tau, Milan, Italy;* [3]*Department of Physiology, University of Tuebingen, Tuebingen, Germany;* [4]*Institute of Anatomy and Physiology, University of Zurich, Zurich, Switzerland;* [5]*Chair of Nephrology, Ateneo Vita e Salute, S. Raffaele Hospital, Milan, Italy;* [6]*Department of Pharmacology, Paracelsius Medical University, Salzburg, Austria; and* [7]*Department of Biomolecular Sciences and Biotechnology, Free University of Milan, Milan, Italy*

Submitted 22 July 2007; accepted in final form 6 May 2008

Capasso G, Rizzo M, Garavaglia ML, Trepiccione F, Zacchia M, Mugione A, Ferrari P, Paulmichl M, Lang F, Loffing J, Carrel M, Damiano S, Wagner CA, Bianchi G, Meyer G. Upregulation of apical sodium-chloride cotransporter and basolateral chloride channels is responsible for the maintenance of salt-sensitive hypertension. *Am J Physiol Renal Physiol* 295: F556–F567, 2008. First published May 14, 2008; doi:10.1152/ajprenal.00340.2007.—We investigated which of the NaCl transporters are involved in the maintenance of salt-sensitive hypertension. Milan hypertensive (MHS) rats were studied 3 mo after birth. In MHS, compared with normotensive strain (MNS), mRNA abundance, quantified by competitive PCR on isolated tubules, was unchanged, both for Na^+/H^+ isoform 3 (NHE3) and Na^+-K^+-$2Cl^-$ (NKCC2), but higher (119%, $n = 5$, $P < 0.005$) for Na^+–Cl^- (NCC) in distal convoluted tubules (DCT). These results were confirmed by Western blots, which revealed: *1*) unchanged NHE3 in the cortex and NKCC2 in the outer medulla; *2*) a significant increase (52%, $n = 6$, $P < 0.001$) of NCC in the cortex; *3*) α- and β-subunit channels [epithelial Na^+ channel (ENaC)] unaffected in renal cortex and slightly reduced in the outer medulla, while γ-ENaC remained unchanged. Pendrin protein expression was unaffected. The role of NCC was reinforced by immunocytochemical studies showing increased NCC on the apical membrane of DCT cells of MHS animals, and by clearance experiments demonstrating a larger sensitivity ($P < 0.001$) to bendroflumethiazide in MHS rats. Kidney-specific chloride channels (ClC-K) were studied by Western blot experiments on renal cortex and by patch-clamp studies on primary culture of DCT dissected from MNS and MHS animals. Electrophysiological characteristics of ClC-K channels were unchanged in MHS rats, but the number of active channels in a patch was 0.60 ± 0.21 ($n = 35$) in MNS rats and 2.17 ± 0.59 ($n = 23$) in MHS rats ($P < 0.05$). The data indicate that, in salt-sensitive hypertension, there is a strong upregulation, both of NCC and ClC-K along the DCT, which explains the persistence of hypertension.

type 3 sodium/hydrogen exchanger; sodium-potassium 2 chloride cotransporter; sodium-chloride cotransporter; epithelial sodium channel; kidney-specific chloride channel; pendrin; aldosterone

HYPERTENSION IS THE MOST IMPORTANT risk factor for diseases of several organs, including heart, brain, and kidney. Despite the impressive number of studies, the etiology of hypertension is still incompletely understood. However, in recent years, it has become increasingly clear that the kidney may play an important role in both the induction and maintenance of salt-sensitive hypertension. Accordingly, hypertension can be induced by transplanting kidneys from genetically hypertensive rats into normotensive control rats (5). More importantly, mutations of genes, encoding proteins expressed in the kidney and involved in tubular ion transport, are associated with modifications of systemic blood pressure. For instance, loss of function mutations of ion transport molecules lead to Bartter's or Gitelman's syndrome (37), characterized by urinary sodium and chloride loss, resulting in orthostatic hypotension. In contrast, gain of function mutations of amiloride-sensitive sodium channels causes Liddle's syndrome, which is phenotypically characterized by systemic hypertension (39). Finally, mutations in the WNK1 and WNK4 genes, two members of the WNK family, are linked to pseudohypoaldosteronism type II (PHA II; also known as familial hyperkalemic hypertension or Gordon's syndrome), which is characterized by a thiazide-sensitive hypertension and hyperkalemia (28).

Studies in animal models for genetic hypertension have also highlighted the importance of the kidney in the development and maintenance of hypertension (10). In particular, in the rat Milan hypertensive strain (MHS), hypertension develops because of a primary alteration in renal tubular Na^+ reabsorption (4), linked to increased activity and expression of Na^+-K^+-ATPase (31), eventually induced by point mutations of adducin (42), a cytoskeletal protein involved in actin polymerization and cell signal transduction (20). Recently, it has been demonstrated that, in these strains of rats, there is a deficient endocytosis of the sodium pump that, by affecting the time that this molecule resides in the plasma membrane, may be an important contributing factor for the increased capacity of the renal tubule cells to reabsorb sodium (13). Therefore, the importance of the Na^+-K^+-ATPase in the pathogenesis of hypertension is fully established (3).

However, while in these strains of rats the exit step has been very well investigated, the entry of Na^+ into the cell across the luminal membrane of renal tubules (a prerequisite for active transcellular Na^+ reabsorption) has not been adequately addressed. Recently, we have demonstrated that Na^+ entry is increased during the induction phase of hypertension in young

Address for reprint requests and other correspondence: G. Capasso, Chair of Nephrology, Second Univ. of Napoli, Nuovo Policlinico, Padiglione 17, Via Pansini 5, 80131 Napoli, Italy (e-mail: gb.capasso@unina2.it).

The costs of publication of this article were defrayed in part by the payment of page charges. The article must therefore be hereby marked "*advertisement*" in accordance with 18 U.S.C. Section 1734 solely to indicate this fact.

0363-6127/08 $8.00 Copyright © 2008 the American Physiological Society

Downloaded from ajprenal.physiology.org on April 27, 2009

MHS animals, paralleled by an upregulation of the Na^+-K^+-$2Cl^-$ cotransporter (NKCC2) at the level of the thick ascending limb (TAL) (9).

Here we set out to study the mechanisms involved in maintaining hypertension in these rats after adolescence. To this end, we examined at the transcriptional and translational levels the most important apical membrane transporters expressed in the various tubular segments of the nephron, i.e., the type 3 sodium/hydrogen exchanger (NHE3) in the proximal tubule (PT), the bumetanide-sensitive NKCC2 in the TAL of Henle's loop, the thiazide-sensitive sodium-chloride cotransporter (NCC) in the distal convoluted tubule (DCT), the epithelial Na^+ channel (ENaC) in the connecting tubule (CNT) through the cortical collecting duct (CCD), and the chloride/bicarbonate exchanger, pendrin. With respect to the last transporter, in the kidney it has been localized in the intercalated cell type B, and in intercalated cell type non-A-non-B of CCD and CNT (45). Recently, it has been hypothesized that this new pathway for transcellular chloride absorption may be implicated also in the control of electrolyte homeostasis and eventually blood pressure. These reports prompt us to investigate the role of pendrin in the Milan hypertensive model of hypertension (45). Finally, since NCC and ENaC have been shown to be sensitive to the effect of aldosterone (24, 30), we have also measured the plasma level of this hormone.

We present data demonstrating that the NCC gene transcript, measured in DCT, and the related protein abundance, also at the level of apical membrane, are significantly increased in MHS. These changes are confirmed by a larger sensitivity to bendroflumethiazide (BTZ) in the same animals. Since at this level the basolateral exit step for chloride is presumed to occur via kidney-specific chloride channels (ClC-K), we measured the abundance and the activity of ClC-K in renal cortex and in primary culture of DCT isolated from MNS and MHS animals. The Western blot experiments and the patch-clamp studies showed increased ClC-K density, without any appreciable alteration of biophysical channel characteristics.

These results suggest that the expression and activity of both the apical (NCC) transporters and basolateral (ClC-K) channels expressed in DCT of MHS animals are upregulated, thus identifying this segment as the site of increased sodium chloride reabsorption and explaining the salt sensitivity of this form of hypertension. This hypothesis is further confirmed by the data showing that the two other apical transporters expressed downstream to the DCT, i.e., the ENaC and pendrin, are downregulated or unaffected, respectively, in MHS animals.

METHODS

The experiments were performed on MHS and Milan normotensive strain (MNS) of rats (generously provided by Prassis Research Institute), aged 85–87 days, and maintained on a standard diet containing 0.5% NaCl. All animal studies were according to animal welfare laws. All the investigations involving animals were conducted in conformity with the *Guiding Principles in the Care and Use of Laboratory Animals* of the American Physiological Society and were approved by the Ethical Committee of the Second University of Naples.

Tubule microdissection. After anesthesia (Ketamin 60 mg/kg body wt plus xylazine 10 mg/kg), the left kidney was removed and washed in ice-cold dissection solution containing the following (in mM): 137 NaCl, 5.4 KCl, 25 $NaHCO_3^-$, 0.3 Na_2HPO_4, 0.4 KH_2PO_4, 0.5 $MgCl_2$, 10 HEPES, 5 glucose, and 1 glycine. PT and medullary TALs were isolated according to the method described earlier by Schafer et al. (36). Small pieces of renal cortex (for PT) and inner stripe of outer medulla (for TAL) were cut under the stereomicroscope and incubated for 30 min at 37°C in the microdissection solution containing 0.5 mg/ml collagenase, continuously bubbled with 95% O_2–5% CO_2. After the digestion, the tissues were washed with ice-cold collagenase-free dissection solution, containing 1 g/l albumin. PTs were isolated free hand from renal cortex under the stereomicroscope. TALs were separated from other cells and fragments by filtering the supernatant through an 80-μm opening nylon mesh (Millipore). For the distal tubules (DT), the starting material was a small piece of renal cortex; the tubules were identified and dissected under scope.

Whole kidney clearance. The rats were anesthetized with an intraperitoneal injection of Inactin, 120 mg/kg body wt, tracheostomized, placed on a thermo-regulated table (37°C), and prepared for renal clearance evaluation. In brief, the right carotid artery was catheterized to monitor blood pressure through a blood pressure recorder (BP1 by WPI) and to take blood samples for inulin concentration measurements. The left jugular vein was cannulated with polyethylene PE-50 tubing and used for intravenous infusion via a syringe pump (Braun, Melsungen) of 0.74 mg·100 g body wt^{-1}·$min\ inulin^{-1}$. To prevent dehydration, the perfusion pump was adjusted to deliver 3.8 ml/h of saline solution. The surgical procedure also included bladder catheterization with PE-50 tubing. After a 60-min equilibration period, the first of seven 30-min urine collections began. After two control clearances, BTZ (200 μg dissolved in 200 μl saline) was injected intravenously as a bolus. Arterial blood samples (100 μl) were taken at the start and end of each collection period. Inulin concentrations in plasma and urine were measured by colorimetric method, while Na^+ and Cl^- were measured by an electrolyte analyzer (Nova Biomedical). Glomerular filtration rate (GFR) was calculated using standard clearance formulae.

Molecular biology experiments. The mRNA abundance of the various transport proteins was performed as previously reported (9). In short, total RNA (0.5–2 μg) was purified from isolated tubules. After isolation, the tubules were transferred into 350 μl of lysis buffer containing guanidinium isothiocyanate and β-mercaptoethanol. The lysate material was loaded on a silica gel membrane (Qiagen) that was washed three times. The concentration and purity of RNA were determined by measuring its absorbance at 260 and 280 nm using a GeneQuant RNA/DNA calculator (Pharmacia Biotechnology).

For the reverse transcription, cDNA was synthesized from equal amounts of total RNA (100–200 ng) using the following: 200 units murine leukemia virus reverse transcriptase (GIBCO BRL); 0.5 μg of $oligo(dT)_{12-18}$ (GIBCO, BRL); 10 mM dithiothreitol; and 2.5 mM dNTP (Pharmacia) in a total volume of 20 μl.

PCR reactions were performed in a total volume of 50 μl in the presence of the following: 10 pmol of each oligonucleotide primer, 200 μM dNTP solution, 5 μl of 10× PCR buffer, 1.5 mM $MgCl_2$, and 1.25 units Taq polymerase. For NHE3, the following primers were used: 5′ ACCACGTCCAGGATCCATACA 3′ (sense) and 5′ CACGAAGAAGGACACTATGCC 3′ (antisense). For NKCC2, the sequence of primer sense was 5′ GGCCTCATATGCG CTTATTA 3′, whereas the antisense was 5′ AGTGTTTGGCTTCATTCTCC 3′. Finally for NCC, a PCR product of 550 bp was obtained using the following primers: 5′ AAGTCGGGTGGTACCTATTT 3′ (sense) and 5′ CAGAAAATGGCCATGAGTGT 3′ (antisense). Samples were denatured at 95°C for 3 min, followed by 33 cycles consisting of denaturing at 95°C (1 min), annealing at 65, 60, and 58°C (30 s) for NHE3, NKCC2, and NCC, respectively, and extension at 72°C (1 min).

The cDNA, synthesized as described before, was utilized for the internal standard synthesis. For the NHE3 internal standard, the NHE3 sense primer and the NHE3 linker antisense primer (5′ GGACACTATGCCGTCACCGCGTCATTAA 3′) were used. The PCR product was reamplified utilizing the NHE3 sense and antisense primers. For NKCC2 internal standard synthesis, NKCC2 sense primer and a linker antisense primer (5′ GCTTCATTCTCCTGTTCTTCATCAGCC 3′)

Downloaded from ajprenal.physiology.org on April 27, 2009

were utilized. A second amplification was performed using the normal NKCC2 sense and antisense primers. For the synthesis of NCC internal standard, the cDNA was amplified using the following primers: NCC sense primer and 5′ GCCATGAGTGTTGGAGAACATC-CCGAAGAA 3′ (linker antisense). The PCR product was reamplified utilizing the sense and antisense NCC primers.

For each mRNA quantification, competitive PCR reactions were performed using as templates the cDNA obtained from total RNA, extracted from the various tubular segments, and the corresponding internal standards. Five to eight competitive PCRs were performed by addition of decreasing amounts of the competitive template (internal standard) to replicate reactions containing identical amounts of cDNA. A progressive decrease of the competitive template PCR product corresponds to a progressive increase of the wild-type template PCR product. Results are expressed per nanogram (ng) of total RNA.

Western blot analysis of NHE3, NKCC2, NCC, ENaC subunits, ClC-K, and pendrin. Thin pieces (100–200 mg) of renal cortex (for NHE3, NCC, ENaC subunits, ClC-K, and pendrin) and of inner stripe of outer medulla (for NKCC2 and ENaC subunits) were frozen at −80°C and then disrupted with a potter homogenizer at 4°C in membrane buffer (150 mM NaCl, 50 mM Tris·HCl, 5 mM EDTA + 10% SDS) containing the following (in μg/ml): 50 4-(2-aminoethyl)-benzenesulfonyl fluoride, 2 leupeptin, and 2 aprotinin. After the centrifugation at 10,000 *g* for 15 min at 4°C, the protein concentration of the supernatant was determined by Bradford assay.

To evaluate the abundance of NHE3, NKCC2, NCC, ENaC subunits, ClC-K, and pendrin, 30 μg of proteins were diluted in 5× loading buffer (10 g/l SDS, 10% glycerol, 1% 2-mercaptoethanol, 5 mM Tris·HCl, pH 6.8), boiled for 5 min, and separated on two 8% SDS-PAGE. After electrophoresis, the first gel was stained with Coomassie blue, and the second gel was submitted to electroblotting to transfer the proteins onto a polyvinylidene difluoride membrane that was washed with phosphate-buffered saline (PBS). After the wash, the membrane was incubated with blocking buffer (2 g/l high purified casein, 1 g/l Tween 20 in PBS) for 1 h and then probed for 1 h with the antibody. Secondary goat anti-rabbit IgG + IgM alkaline phosphatase conjugate was diluted 1:5,000 in 5 ml of blocking buffer and added for 1 h, after two washes in 20 ml of blocking buffer. The last washing was performed three times with 20 ml of blocking buffer, and finally detection was obtained with a CSPD chemiluminescent substrate (Tropix, Bedford, MA). To test for equal loading of proteins (30 μg), anti-β-actin antibody (Sigma Aldrich) diluted 1:1,000 or 0.5% Ponceau S in acetic acid were used. NHE3, NKCC2, NCC, α-ENaC, β-ENaC, γ-ENaC, ClC-K, pendrin, and β-actin abundances in the various nephron segments of MNS and MHS rats were quantified by densitometric analysis. Results are expressed as optical density.

Immunohistochemistry. Kidneys were fixed by vascular perfusion with 3% paraformaldehyde in 0.1 M phosphate buffer. After freezing in liquid propane, kidneys were sectioned in a cryostat. Five-micrometer-thick cryosections were incubated with affinity-purified rabbit anti-NCC antibody (1:12,000) (27) overnight at 4°C. Binding sites of the primary antibody were revealed with a Cy3-conjugated goat-anti-rabbit antiserum (1:1,000; Jackson Immuno Research Laboratories, West Grove, PA). Fluorescent images were acquired with a Leica DFC490 charged-coupled device camera attached to a Leica DM 6000 fluorescence microscope (Leica, Wetzlar, Germany) using corresponding camera parameters for kidneys from normo- and hypertensive rats. We are well aware that immunohistochemistry is not a good method to assess protein abundance. By no means is this method quantitative. However, it may nicely confirm the more quantitative immunoblotting data and may give additional information about axial differences along the nephron and about the subcellular distribution.

Antibodies. We used previously well-characterized rabbit polyclonal antibodies (dilution used in parentheses) to the following proteins: NHE3 (1:5,000), NKCC2 (1:1,000), and NCC (1:1,000). They were provided by Orson Moe (1), Steve Hebert (23), and David Ellison (6), respectively. For α-ENaC (1:5,000), commercially available polyclonal rabbit antibodies were used (Sigma-Aldrich, St. Louis, MO). β- and γ-ENaC (1:5,000) antibodies were provided by Bernard Rossier (11). Antibodies against pendrin (1:5,000) were previously characterized (P. Hafner, R. Grimaldi, P. Capuano, G. Capasso, C. A. Wagner, unpublished observations). For ClC-K (1:200), commercially available antibodies were purchased from Alomone Antibodies (Israel) or Santa Cruz Biotechnology.

Patch-clamp, Western blot, and immuocytochemical studies on primary culture of DCT. DCT tubules were isolated according to the Schafer method (36). Briefly, kidneys were removed from anesthetized rats and placed in ice-cold PBS. After renal capsule removal, sections of 1-mm thickness were cut from the cortical surface opposite to the hilus. Small cortical pieces were incubated in 2 ml of 0.1% (wt/vol) collagenase MEM solution at 37°C for 35 min. The supernatant was placed in a cold test tube, and the tubules were allowed to settle. The supernatant was removed and replaced with 2 ml of cold PBS containing 1% BSA. Sorting has been done by visual inspection using a stereomicroscope. Tubules were placed in multiwells in the presence of the following: RPMI-1640, 5% fetal bovine serum, 5 μg/ml transferrin, 5 μg/ml insulin, 50 nM dexamethasone, 5 pM triiodothyronine, 100 U penicillin, and 0.1 mg/ml streptomicin. Cells, maintained in an incubator at 37°C at the presence of 95% air and 5% carbon dioxide, were allowed to grow for 4 days. After this period of time, cells had still not reached a confluent condition. DCT specificity of the cultured cells was assessed by immunocytochemical experiments, in which NCC expression was confirmed. The specificity of the immunocytochemical procedure was validated by negative controls on WI-26VA4 pulmonary cells (7).

Patch-clamp experiments were performed as previously reported (32). The patch pipette resistance was 5–10 MΩ, and seal resistance was 5–10 GΩ. Potential differences are expressed as overall potential differences, considering the junction potential, the holding potential, and the cell membrane potential, measured to be about −35 mV (current clamp experiments). In cell-attached configuration, the bath solution was an HBSS solution. The micropipette solution (cell-attached and inside-out configurations) contained the following (in mM): 115 *N*-methyl-D-glucamine chloride, 30 tetraethylammonium chloride, 2 $CaCl_2$, 1 $MgCl_2$, and 10 HEPES (pH 7.4). In inside-out configuration, the bath symmetric solution contained the following (in mM): 145 *N*-methyl-D-glucamine chloride, 0.3 $CaCl_2$, 3 EGTA, and 10 HEPES (pH 7.4 or 6 as mentioned). Data analysis was performed by Bruxton Tac program.

In the not confluent cultured cells, ClC-K, which are expressed only on the basolateral membrane in the intact epithelium, were delocalized on the whole cells surface, as yet observed for other ion channels of epithelial cells growing on plastic surface, allowing the feasibility of patch clamp experiments. The expression and localization of ClC-K has been verified by means of immunocytochemical experiments in which layers of cells (60–70% confluency) plated on glass coverslips were fixed with 4% paraformaldehyde and permeabilized with 0.1% Triton X-100. Nonspecific binding was blocked with 5% BSA. Cells were then incubated at the presence of the anti-ClC-K (CLC-K, V-15) (Santa Cruz Biotechnology) primary antibody at room temperature for 1 h, followed by Cy2 anti-goat (1:400 dilution, at room temperature for 1 h) secondary antibody incubation (Jackson Laboratories). Immunofluorescence experiments performed to detect NCC expression in DCT cells have been carried out as above using an anti-NCC antibody (kindly provided by D. Ellison) and a Cy2 anti-rabbit as secondary antibody. Both ClC-K and NCC images were acquired by using a confocal microscope Leica TCS SP2 AOBS (Leica Microsystem, Heidelberg, Germany) with UV lens FW lens ×63 oil 405-nm objective.

Western blot experiments were performed using three confluent layers of DCT cells from plates with a diameter of 6 cm. Total protein was extracted in lysis buffer (60 mM Tris·HCl, pH 6.8, 10% SDS, 15

Downloaded from ajprenal.physiology.org on April 27, 2009

mg/ml DTT, 0.2 mM protease inhibitor cocktail). Cells pelleted from three petri dishes (6 cm diameters) were resuspended in lysis buffer and sonicated for 10 min. Protein concentration was measured by the amido black method. After dilution of 25 μg of proteins in diluted 5× loading buffer (0.3125 M Tris, pH 6.8, 10% SDS, 50% glycerol, 0.005% bromophenol blue, 25% 2-mercaptoethanol), proteins were resolved on a 10% SDS-polyacrylamide gel and electrophoretically transferred to Immuno-Blot polyvinylidene difluoride membranes, which were blocked with 5% nonfat dried milk in Tris-buffered saline (TBS)-Tween (150 mM Tris, pH 7.5, 150 mM NaCl, 0.1% Tween 20) and incubated overnight at 4°C at the presence of a polyclonal antibody against ClC-K (1:200) in TBS plus 5% nonfat dry milk. The bound antibody was detected by the enhanced chemiluminescence (Amersham) using horseradish peroxidase-conjugated anti-goat IgG diluted 1:5,000 in TBS plus 5% nonfat dried milk. Densitometric analysis was performed using ImageJ (National Institutes of Health). Gel loading and transfer procedure were checked by observation of gel and membrane after exposition to Coomassie blue and amido black, in that order.

Plasma aldosterone measurements. For aldosterone measurements, rats were anesthetized by ether, the abdomen was opened, and blood was drawn from the abdominal aorta. Blood collection was interrupted as soon as dyspnea appeared. Plasma aldosterone concentrations were determined using a commercially available radioimmunoassay kit (ALDOCTK-2 dia Sorin cod. P2714, Italy).

Statistical analysis. All data are expressed as means ± SE. Statistical significance was analyzed by means of Prism software (Graph Pad) and was determined as $P < 0.05$ using Student's *t*-test, one-way or two-way ANOVA test, as indicated.

RESULTS

The table in Fig. 1 compiles the data on mean arterial blood pressure, GFR, electrolytes, and aldosterone plasma levels obtained in anesthetized rats. As expected, there was a significant difference in systemic blood pressure and aldosterone plasma levels between the two strains of rats, thus confirming previous results (29). No changes were detected in renal hemodynamic (GFR) and electrolytes plasma levels.

Figure 1, *bottom*, shows the effects of BTZ (200 μg) on Na^+ and Cl^- excretion in MNS and MHS animals. Na^+ excretion in MNS animals was 0.49 ± 0.01 μmol/min ($n = 5$) under basal conditions and 4.16 ± 1.01 μmol/min ($n = 5$) following BTZ administration ($P < 0.05$), whereas in MHS it was 0.78 ± 0.17 μmol/min ($n = 5$) and 9.02 ± 1.31 μmol/min ($n = 5$) ($P < 0.005$), respectively. With respect to Cl^- excretion, in MNS rats it was 1.72 ± 0.29 μmol/min under basal condition and 8.34 ± 0.96 μmol/min after BTZ infusion ($P < 0.005$), whereas in MHS it was 1.79 ± 0.41 and 13.60 ± 1.03 μmol/min ($P < 0.005$), respectively. Therefore, in the first 30 min after the administration, BTZ induced a larger excretion of Na^+ and Cl^- in the hypertensive animals, thus demonstrating

Parameter	MNS	MHS
n	11	11
Body weight (g)	350 ± 6	364 ± 5
MBP (mmHg)	139 ± 1.5	167 ± 1.7 ***
GFR (ml.min^{-1}.100 g. b.w.)	0.84 ± 0.04	0.81 ± 0.04
Plasma Na^+ (mMol)	148.4 ± 1.2	146.7 ± 1.3
Plasma K^+ (mMol)	4.02 ± 0.08	3.89 ± 0.14
Aldosterone (ng.dl^{-1})	6.9 ± 2.6	39.7 ± 5.0 ***

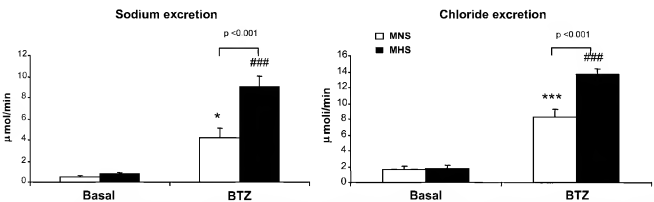

Fig. 1. *Top:* table shows summary of baseline, hemodynamic, electrolytes, and hormonal data in each group of rats. MNS, Milan normotensive rats; MHS, Milan hypertensive rats; *n*, number of animals; MBP, mean blood pressure; GFR, glomerular filtration rate. ***$P < 0.001$ vs. MNS rats. *Bottom:* sodium (*left*) and chloride (*right*) excretion before and 30 min after intravenous infusion of bendroflumethiazide (BTZ) (200 μg). *$P < 0.05$, ***$P < 0.005$, ###$P < 0.005$ vs. the corresponding basal excretion.

Downloaded from ajprenal.physiology.org on April 27, 2009

that these animals are more sensitive to thiazide diuretics. No change were found for blood hematocrit (data not shown), indicating that the acute diuretic administration did not induce extracellular volume contraction.

mRNA and protein abundance of NHE3, NKCC2, and NCC. Using the technique of competitive PCR, we examined whether NHE3 mRNA was different in the two strains of MNS and MHS rats. The quantification was performed on PT, and, for each experiment, the MNS and MHS kidneys were studied in parallel. As shown in Fig. 2, *top*, NHE3 mRNA abundance was not significantly different in PT of MNS rats (0.54 ± 0.13 fmol/ng total RNA, $n = 10$) compared with PT of MHS rats (0.51 ± 0.15 fmol/ng total RNA, $n = 10$).

NHE3 protein abundance was determined by Western blot analysis. As shown in Fig. 2, *middle*, the antibody recognized a protein with a molecular mass between 66 and 116 kDa. Densitometric analysis (Fig. 2, *bottom*) demonstrates that NHE3 abundance, normalized for β-actin, was similar in the two strains (MNS: 0.92 ± 0.06, $n = 9$; MHS: 0.96 ± 0.17, $n = 9$), thus confirming, at protein level, the data of the competitive PCR.

NHE3 mRNA abundance was also measured in TAL. It was again similar in MNS (2.19 ± 0.23 fmol/ng total RNA, $n = 10$) as in MHS (1.80 ± 0.24 fmol/ng total RNA, $n = 10$). The same was found for NHE3 protein abundance, which, normalized for β-actin, was 1.28 ± 0.22 in MNS ($n = 5$) and 1.36 ± 0.31 in MHS animals ($n = 5$).

As shown in Fig. 2, *top*, NKCC2 mRNA abundance was not significantly different in TAL of MNS rats (0.25 ± 0.07 fmol/ng total RNA, $n = 8$) from TALs of MHS (0.16 ± 0.02 fmol/ng total RNA, $n = 8$).

Similarly, NKCC2 protein abundance, as determined by Western blot analysis using outer medulla (Fig. 2, *middle*) was again not significantly different in TAL of MNS animals (2.06 ± 0.08, $n = 5$) compared with TAL of MHS rats (2.19 ± 0.05, $n = 5$).

The results of the competitive PCR reactions for NCC are shown in Fig. 2, *top*. NCC mRNA abundance was significantly ($P < 0.005$) increased in DCT of MHS rats (0.70 ± 0.10 fmol/ng total RNA, $n = 5$) compared with DCTs from MNS rats (0.32 ± 0.03 fmol/ng total RNA, $n = 5$).

Western blot analysis performed on slices from renal cortex (Fig. 2, *middle*) showed that NCC antibody recognized a protein with a molecular mass between 116 and 205 kDa. As illustrated in Fig. 2, *bottom*, densitometric analysis demonstrated that NCC abundance, normalized for β-actin, was

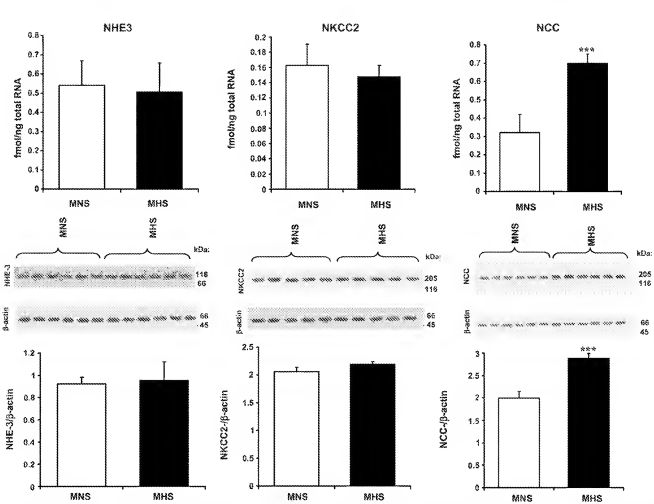

Fig. 2. *Top*: mRNA abundance of type 3 sodium/hydrogen exchanger (NHE3) in proximal tubules, sodium-potassium 2 chloride cotransporter (NKCC2) in medullary thick ascending limbs of Henle's loop, and sodium-chloride cotransporter (NCC) in distal convoluted tubules (DCTs) of 3-mo-old MNS vs. MHS rats. Western blot (WB) results (*middle*) and corresponding protein abundance (*bottom*) of NHE3 in renal cortex, NKCC2 in the outer medulla, and NCC in renal cortex are shown. ***$P < 0.005$.

Downloaded from ajprenal.physiology.org on April 27, 2009

significantly ($P < 0.001$) higher in MHS rats (3.02 ± 0.43, n = 6) compared with MNS animals (1.99 ± 0.15, n = 6).

ENaC subunit protein abundance in kidney cortex and outer medulla. Western blot analysis performed on slices from renal cortex (Fig. 3) showed that α-, β-, and γ-ENaC antibodies recognized proteins with molecular masses between 66 and 116 kDa. As illustrated in Fig. 3, *top*, densitometric analysis demonstrated that α-ENaC abundance, normalized for β-actin, was not different in MNS rats (0.88 ± 0.04, n = 5) from MNS animals (0.87 ± 0.03, n = 5). Similarly, β-ENaC remained unchanged (1.44 ± 0.01, n = 5, in MNS and 1.35 ± 0.03, n = 5, in MHS) (Fig. 3, *middle*). The same was observed for γ-ENaC (0.79 ± 0.02, n = 5, in MNS and 0.81 ± 0.05, n = 5, in MHS) (Fig. 3, *bottom*).

Similar results were obtained in the inner stripe of the outer medulla (Fig. 3), where α-ENaC abundance was modestly reduced (0.98 ± 0.04) (n = 5) in MHS compared with 1.17 ± 0.02 (n = 5) in MNS animals ($P < 0.05$) (Fig. 3, *top*). Also, β-ENaC was slightly reduced ($P < 0.05$) in MHS (0.62 ± 0.01, n = 5) vs. MNS animals (0.69 ± 0.02, n = 5) (Fig. 3, *middle*). γ-ENaC was unchanged: 0.52 ± 0.03 (n = 5) in MNS vs. 0.50 ± 0.03 (n = 5) in MHS (Fig. 3, *bottom*).

Immunocytochemistry of NCC. Figure 4 shows NCC immunofluorescence staining of tissue sections. Immunofluorescent staining is much stronger in the renal cortex of hypertensive than in normotensive rats. High magnifications (Fig. 4, *bottom*) reveal that both groups of rats exhibit apical localization of NCC in the DCTs. These results confirm and reinforce the competitive PCR and the Western blot data, indicating that NCC, in MHS, may be implicated in increased salt reabsorption.

Pendrin protein abundance. Western blot analysis performed on slices from renal cortex (Fig. 5) showed that pendrin antibodies recognized a protein with a molecular mass around 120 kDa. As illustrated in Fig. 5, densitometric analysis demonstrated that pendrin abundance, normalized for β-actin, remained unchanged in MHS rats (0.59 ± 0.1, n = 5) compared with that in MNS animals (0.68 ± 0.1, n = 5).

ClC-K protein abundance. The main route for Cl^- exit at the level of the DTs is through ClC-K. To explore, whether the enhanced expression of the Cl^- entry mechanism NCC in MHS animals is paralleled by a similar increase of the Cl^- exit mechanism ClC-K, we performed Western blot experiments to measure the protein abundance of ClC-K. The results are reported in Fig. 6. ClC-K protein abundance in kidney cortex, normalized for β-actin, was significantly ($P < 0.005$) increased in MHS animals (1.09 ± 0.06, n = 5) compared with MNS rats (0.85 ± 0.07, n = 5).

Chloride channel activity recorded by patch-clamp experiments. To characterize chloride channels of DCT cells and to evaluate the contribution of the ClC-K and its possible functional modifications, DCT cells were taken into primary culture

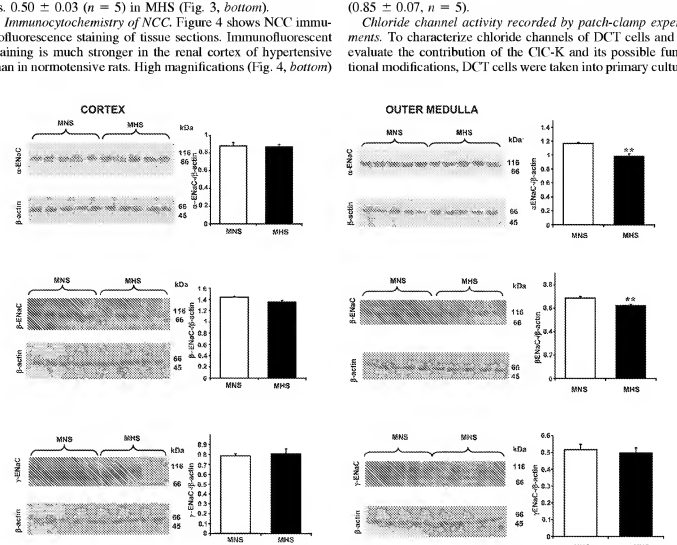

Fig. 3. *Left*: α-epithelial Na^+ channel (ENaC), β-ENaC, and γ-ENaC protein abundance in the renal cortex from kidneys of 3-mo-old MNS and MHS animals, as detected by WB. *Right*: α-ENaC, β-ENaC, and γ-ENaC protein abundance in the inner stripe of the outer medulla from kidneys of 3-mo-old MNS and MHS animals as detected by WB. $^{**}P < 0.01$.

Downloaded from ajprenal.physiology.org on April 27, 2009

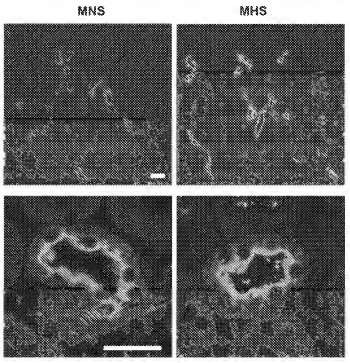

Fig. 4. Detection of thiazide-sensitive NCC in kidneys of MNS (*left*) and MHS (*right*) rats (representative picture of a single experiment, $n = 5$). Immunofluorescent staining is much stronger in the renal cortex of MHS than in MNS rats. High magnifications (*bottom*) reveal that both groups of rats exhibit apical localization of NCC in the DCTs. Immunofluorescence on cryosections of phosphonoformic acid-fixed kidneys using previously characterized, affinity-purified antibodies against NCC is shown. Bars ~50 μm.

and used for electrophysiological measurements. DCT specificity of the cultured cells was assessed by immunocytochemical experiments, in which NCC expression was confirmed (data not shown). NCC distribution on the whole cell surface is in agreement with the loss of polarity of used cells. The specificity of the immunocytochemical procedure was validated by negative controls on TAL cultured cells. By means of patch clamp in the cell-attached configuration, a channel showing outward rectification and single channel conductance (G) of 30.3 ± 4.3 pS at +65 mV and 15.5 ± 3.5 pS at −135 mV ($n = 7$) was detected in 24% of total seals obtained in cultured DCT MNS cells (Fig. 7, *A* and *B*). The channel open probability (Po) was significantly reduced at hyperpolarized voltages, and it was 0.63 ± 0.07 and 0.18 ± 0.08 ($n = 7$) at +65 mV and −135 mV, respectively ($P < 0.01$, one-way ANOVA). The current reversal potential was −44.6 ± 5.9 mV ($n = 7$), well in agreement with the one expected for a chloride channel. Calculated chloride intracellular activity was ~20 mM, as previously reported in kidney epithelial cells (15). In MHS cells, channel rectification, G (G + 65 mV = 27.0 ± 1.7 pS, G − 135 mV = 13.9 ± 2.1 pS; $n = 11$), reversal potential (−58.1 ± 4.4 mV; $n = 11$), and Po (0.52 ± 0.09 and 0.06 ± 0.04 at +65 and −135 mV correspondingly) were similar to the respective values in MNS isolated DCT cells (Fig. 7*C*). The channel density (d) (number of active channels in a patch) and activity (calculated as d·Po) were, however, significantly higher in MHS compared with MNS DCT isolated cells (d was 0.60 ± 0.21, $n = 35$, in MNS rats and 2.17 ± 0.59, $n = 23$, in MHS rats with a $P < 0.05$ comparing the two groups by means of the Student's *t*-test; Fig. 7, *D* and *E*).

Crude membrane extracts from DCT kidney cells were analyzed by SDS-PAGE and Western blotting and displayed two bands in the size range 70–110 kDa (Fig. 7*F*). Densitometric analysis of Western blot experiments was performed on the 110-kDa fully glycosylated functional cell membrane protein. In MHS protein preparations, a significant ($P < 0.01$, Student's *t*-test) increase in glycosylated channel expression (d = 30.9 ± 4.2, $n = 7$, in MNS rats, and d = 69.1 ± 4.3 in MHS rats; Fig. 7*G*) was observed in agreement with the higher channel density and activity observed in patch-clamp experiments.

The biophysical characteristics of the MNS and MHS DCT channel resembled those of the ClC-K observed in distal nephron (22). Furthermore, analysis of current traces suggests an apparent channel "double-pore behavior" in which activity bursts, during which the channel opened to two equidistant current levels, are separated by relatively long closures (i.e., indicated in Fig. 8*A* by an arrow), and synchronous opening and closing events (asterisks in Fig. 8*A*) were often present. As values of calculated probability supposing the presence of independent channels differed from the experimentally obtained values, we could assume a pore cooperative behavior. To further characterize channel properties, we performed patch-clamp experiments in inside-out configuration in the presence of symmetric chloride solutions. The channel showed an outward rectification (G + 75 mV = 31.8 ± 9.7 pS, G − 65 mV = 16.7 ± 4.6 pS; $n = 4$) and lack of Po inactivation that

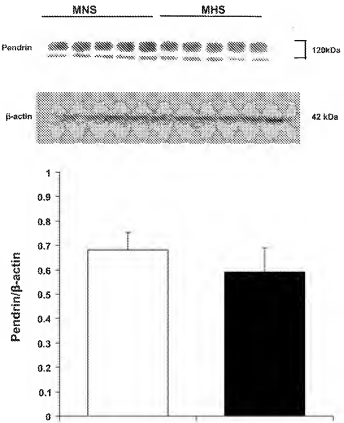

Fig. 5. Pendrin expression in the renal cortex of kidneys from 3-mo-old MNS and MHS animals, as detected by WB ($n = 5$).

Downloaded from ajprenal.physiology.org on April 27, 2009

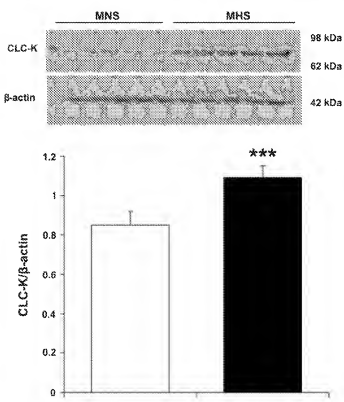

Fig. 6. Kidney-specific chloride channel (ClC-K) protein abundance in the renal cortex of kidneys from 3-mo-old MNS and MHS animals, as detected by WB ($n = 5$). ***$P < 0.005$.

was ~0.4 over the whole range of potentials tested (Fig. 8, *D–F*), as previously observed.

Chloride channels studied by immunofluorescence and Western blot methods. The presence of ClC-K in cultured DCT cells was further confirmed by means of immunocytochemical and Western blot experiments. Primary antibody specificity was proven by Western blots and as a negative control in WI-26VA4 pulmonary cells (data not shown). Secondary antibody specificity was verified by signal deficiency on DCT cell not exposed to the primary ClC-K antibody (data not shown).

DISCUSSION

Previously, our laboratory demonstrated that the induction of the hypertensive process in MHS rats is coupled to the upregulation of the NKCC2 along the TAL (9). In the present study, we investigated the luminal transport proteins that sustain hypertension after adolescence in these rats. First of all, we confirmed that MHS animals were hypertensive, and this was associated with increased aldosterone plasma levels, unchanged GFR, plasma sodium, and potassium (5).

NHE3 mRNA and protein abundance in PTs. Determination of NHE3 mRNA and protein abundance in renal PTs isolated from 3-mo-old MHS and age-matched MNS rats revealed that NHE3 transcript and protein abundance are not significantly different in the two strains of rats, thus indicating that the modulation of NHE3 expression does not seem to be involved in the maintenance of hypertension in the MHS animals. These results are in seeming contrast to a previous report demonstrating that Na^+/H^+ exchanger activity is increased in MHS compared with MNS (18). However, it cannot be excluded that the contribution of the NHE3 gene to the MHS hypertension is mediated by its increased activity, not necessarily associated with an overexpression.

Although NHE3 is not the major sodium transport along the TAL, we have also checked NHE3 mRNA expression and protein abundance in this segment. No difference was found between the two strain of rats.

NKCC2 mRNA and protein abundance along the TAL. NKCC2 gene expression in the TAL is unchanged both at mRNA and protein level in MHS compared with MNS rats. These results are completely different from what our laboratory found in 3-wk-old MHS animals, where a substantial and significant increase in the NKCC2 has been detected (9). It is, therefore, justified to postulate that, in older animals, NKCC2 gene expression normalizes, whereas it is upregulated during the first weeks of life.

NCC expression and activity in the DCT. One major new finding of the present study is the identification of the thiazide-sensitive NCC as a potential player in the maintenance of this form of salt-sensitive hypertension. Indeed, as shown in Fig. 3, NCC gene expression in the DT is significantly enhanced both at mRNA and protein level in MHS rats. These results are fully supported by the immunocytochemistry studies (Fig. 6), showing much stronger staining of NCC antibodies on the apical membranes of DCT of MHS rats. Finally, the larger sensitivity to thiazide diuretic of the same strain of animals (Fig. 7) indicates that, not only the expression, but also the NCC activity, is upregulated in the hypertensive rats. The strong stimulation of the NCC could potentially contribute to the significant rise in blood pressure. Several lines of evidence support this hypothesis: *1*) the DT is an important site of Na^+ transport; actually, roughly 7–10% of the filtered Na^+ load is normally reabsorbed at this level; *2*) apical Na^+ entry in the early part of the DT is mainly mediated by the thiazide-sensitive NCC (26), as demonstrated by the significant natriuresis associated with the use of thiazide diuretics; *3*) patients carrying a mutation with a loss of function of the NCC gene (Gitelman syndrome) are characterized by orthostatic hypotension (8), while patients with PHA II, associated with a functional activation of the NCC, are hypertensive (28); *4*) during aldosterone escape, NCC is downregulated, suggesting that natriuresis is restored by high blood pressure through the cotransporter, despite the continuous presence of a high concentration of aldosterone (47); and *5*) finally and most importantly, patients with salt-sensitive hypertension and carrying α-adducin polymorphism are exquisitely sensitive to hydrochlorotiazide treatment (38). Taken together, these physiological, pharmacological, molecular, and clinical data all indicate that NCC is implicated in primary hypertension. In contrast with the hyperkalemia found in patients with PHA II, plasma potassium is normal in the MHS rats (Fig. 1, *top*). The lack of high plasma K^+ may be related to the larger urine flow rate of MHS compared with the MNS (data not shown). This is an important observation, since we know that K^+ excretion rate is mainly flow dependent (eventually mediated by the maxi-K channels). Therefore, it is entirely possible that hyperkalemia does not develop due to the activation of the flow-dependent K^+ secretion pathway. Indeed, when we measured 24-h K^+ excretion rate, we found that it was significantly increased in MHS compared with MNS (data not shown).

Downloaded from ajprenal.physiology.org on April 27, 2009

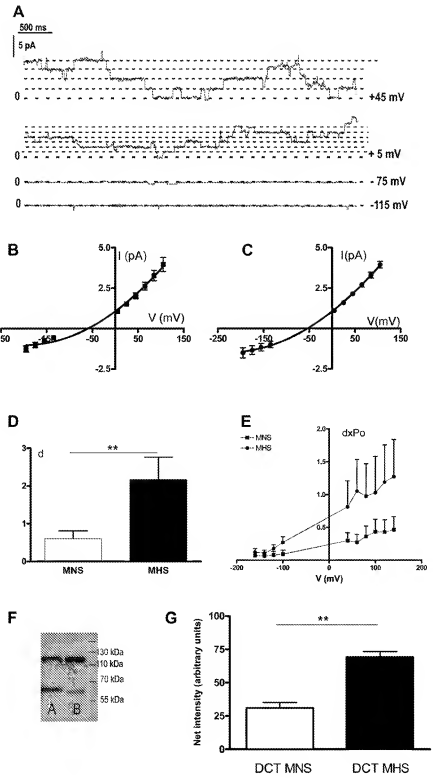

Fig. 7. Chloride channels in MNS and MHS DCT cells. *A*: single-channel current traces of the 30 pS Cl⁻ channel recorded at positive or negative potentials. 0 is the closed channel level. *B*: single-channel current-voltage (*I-V*) relationships for the channel in MNS-isolated DCT cells ($n = 7$). *C*: *I-V* curve for the same channel observed in MHS cells ($n = 11$). *D*: channel density in MNS ($n = 32$) and MHS ($n = 21$) DCT cells (d = channel density, n = number of seals). $^{**}P < 0.01$. *E*: channel activity in MNS ($n = 32$) and MHS ($n = 21$). Po, open probability. *F*: WB analysis of ClC-K expression in DCT (*lane A* = MNS and *lane B* = MHS) cells. *G*: densitometric analysis of WB experiments ($n = 7$). Histograms represent the mean band intensity (arbitrary units) of 7 different membrane preparations. $^{**}P < 0.01$.

NCC and aldosterone. Several hypotheses may be advanced to identify the mechanism(s) responsible for the reported increase in NCC transcription and abundance, but the findings that, in adult MHS animals, plasma aldosterone is significantly elevated (Fig. 1, *top*) may indicate that aldosterone is implicated. Many observations demonstrate that the NCC can be regulated by aldosterone plasma levels. Indeed, by free-flow micropuncture studies, Hierholzer et al. (19) demonstrated that Na^+ reabsorption was largely impaired along the DCT of adrenelectomized rats and was restored by aldosterone administration, a finding that was later confirmed by other investigators using in vivo microperfusion of rat DT (41, 44). More-

Downloaded from ajprenal.physiology.org on April 27, 2009

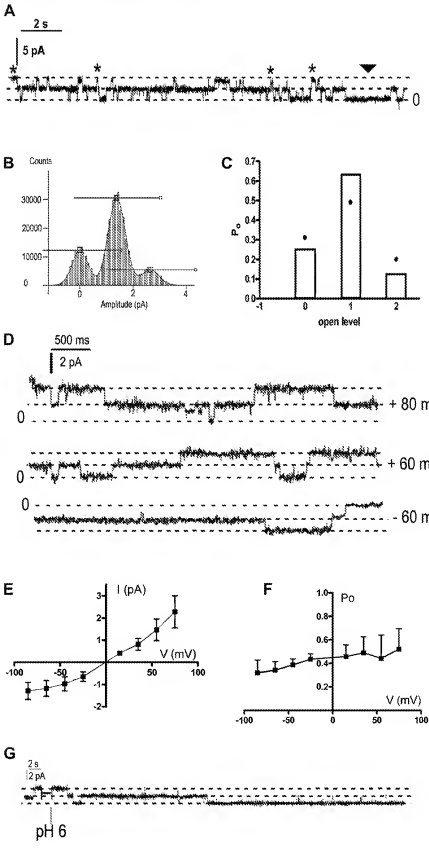

Fig. 8. Single-channel properties of the ClC-K-like channel in MNS DCT cells both in cell-attached (*A–C*) and in inside-out (*D–G*) configuration. *A*: single-channel trace at +45 mV. The arrow indicates a common closure separating burst of channel activity. Asterisks indicate nearly simultaneous opening and closing. The 0 corresponds to closed-channel level. *B*: all point amplitude histograms of currents showed in *A*. The distribution was fitted by a sum of three Gaussian curves. *C*: bars indicate the Po for one closed (0) and two open (1, 2) levels, obtained from the Gaussian fit; solid circles indicated the calculated Po, assuming the presence of two independent channels, each with Po = 0.44. *D*: current traces registered at positive and negative membrane potentials as reported. The 0 corresponds to closed-channel level. *E*: single-channel *I-V* relationships ($n = 4$) recorded at the presence of symmetric chloride solutions. *F*: Po-*V* relationship for this channel in inside-out condition. A slight but not significant decrease of channel Po could be observed at hyperpolarized voltages. *G*: representative current trace showing how exposition to the same bath symmetric solution with acid (pH 6) pH induced a reduction in channel Po.

Downloaded from ajprenal.physiology.org on April 27, 2009

over, aldosterone has been shown to increase both [^{3}H]metolazone binding in membrane fractions from renal cortex (14) and NCC abundance measured by immunoblotting with specific anti-NCC antibodies (25).

ENaC subunits in the collecting ducts. In the present study, we have also examined the expression of ENaC that is the key apical Na^+ channel in the CNT and collecting duct. During active sodium absorption, all three subunits are found mostly in the apical domain of segment-specific cells, whereas, during natriuresis, β- and γ-ENaC are mainly localized in cytosolic vesicles (17). Aldosterone regulates ENaC-dependent Na^+ reabsorption by changing the expression and subcellular localization of the individual ENaC subunits (12, 30). Our present findings indicate that, in the outer medulla of MHS kidneys, there is a modest, although significant, downregulation of the α- and β-subunits, whereas the γ-subunit was not affected. A possible explanation may be related to the reduced Na^+ load that reaches this segment due to the increased reabsorption along the DT, driven by the strong increase in NCC abundance. The observation that ENaC are not upregulated (even in the presence of high aldosterone) is not surprising, since, in other models, like renal outer medullary K channel null mice (a model of type II Bartter syndrome), characterized by very high plasma aldosterone, there is a very significant stimulation of NCC, while the abundance of the α-, β-, and γ-subunits of ENaC is only slightly increased, a finding confirmed by the unchanged fractional volume of CNT and collecting duct (C. Wagner and J. Loffing, personal communication).

Pendrin protein abundance. The expression of the chloride/anion exchanger pendrin (SLC26A4) is restricted to the apical side of type B intercalated cells in the connecting segment and CCD (45). There, pendrin has been implicated in bicarbonate, and it has been described that pendrin expression may be regulated by urinary chloride excretion, which suggested a role in transcellular chloride absorption (35). In particular, pendrin expression is reduced when large amounts of chloride are delivered to the CNT and CCD and is upregulated during chloride depletion. In the present experiments, pendrin abundance was clearly unchanged, and this has two theoretical implications: *1*) this protein is not implicated in the maintenance phase of salt-sensitive hypertension; and *2*) high blood pressure releases the reported correlation between chloride delivery and pendrin abundance.

Chloride channels. NaCl transepithelial transport requires appropriate chloride efflux across the basolateral membrane, which, in the distal nephron, is mainly mediated by ClC-Kb Cl^- channels (22). Immunocytochemestry, RT PCR, and in situ hybridization (33, 43) verified the expression of ClC-K2 in the basolateral membrane of TAL, DCT, CNT, and intercalated cells. The presence, in primary cultures of DCT isolated cells, of a chloride channel whose single-channel biophysical characteristics (current-voltage relationship, G, "double-channel behavior", voltage dependence and independence of Po in cell-attached and inside out, respectively) resemble those of the ClC-Kb observed in the distal nephron (34, 46), is, therefore, well in agreement with the known renal localization of this channel.

The importance of ClC-K2 in NaCl reabsorption is supported by the observation that loss of function mutations of ClC-Kb (the human ortholog of rodent ClC-K2) has been demonstrated in a variant of the Bartter syndrome (40), while a gain of function mutation of the same channel has been found to be related to human hypertension (21). In addition, it has been recently shown that salt-sensitive hypertension may be associated with chloride channel polymorphism (2).

Therefore, our observation of a significant increase in active channel density, but not of other channel biophysical characteristics, in DCT cells of MHS rats is well in agreement with the possibility of an increased transepithelial NaCl flux during the maintenance phase of hypertension. The observed increase of active channel density could be related to a higher ClC-K protein expression in the membrane, as suggested by Western blot experiments. Preliminary patch-clamp data (not reported) allowed us to establish that, in TAL-isolated cells, ClC-K biophysical characteristic, density, and activity were the same in both MHS and MNS rats. Even if other distal nephron segments remain to be analyzed, these preliminary results imply that the density of active ClC-K could increase only in some nephron distal sites.

Conclusions. We have found that, in adult MHS animals characterized by salt-sensitive hypertension, the expression and abundance of NHE3 and NKCC2, measured along the PT and the TAL, are not different, while the NCC, expressed along the cortical DT, is upregulated, probably due to higher plasma aldosterone level.

These last results have been confirmed by clearance experiments demonstrating a larger sensitivity to BTZ in MHS animals, and by immunocytochemical studies showing increased NCC on the apical membrane of DCT cells of the same animals.

The increased entry step for NaCl is matched by a similar upregulation of the chloride conductive pathway, i.e., ClC-K. Finally, in the collecting ducts, there is a modest downregulation of the gene expression and protein abundance of α- and β-ENaC. Therefore, the combined upregulation of NCC and ClC-K along the DT may explain the increase in systemic blood pressure through their action on salt reabsorption that is only partially offset by the downregulation of ENaC (α- and β-subunits).

ACKNOWLEDGMENTS

We thank Orson Moe, Steve Hebert, David Ellison, and Bernard Rossier for providing us with the antibodies used in this study.

GRANTS

This study was supported by a grant from Ministero Ricerca Scientifica (Cofin 2004 and 2006).

REFERENCES

1. **Amemiya M, Loffing J, Lotscher M, Kaissling B, Alpern RJ, Moe OW.** Expression of NHE-3 in the apical membrane of rat renal proximal tubule and thick ascending limb. *Kidney Int* 48: 1206–1215, 1995.
2. **Barlassina C, Dal FC, Lanzani C, Manunta P, Guffanti G, Ruello A, Bianchi G, Del VL, Macciardi F, Cusi D.** Common genetic variants and haplotypes in renal CLCNKA gene are associated to salt-sensitive hypertension. *Hum Mol Genet* 16: 1630–1638, 2007.
3. **Bianchi G.** Genetic variations of tubular sodium reabsorption leading to "primary" hypertension: from gene polymorphism to clinical symptoms. *Am J Physiol Regul Integr Comp Physiol* 289: R1536–R1549, 2005.
4. **Bianchi G, Baer PG, Fox U, Duzzi L, Pagetti D, Giovannetti AM.** Changes in renin, water balance, and sodium balance during development of high blood pressure in genetically hypertensive rats. *Circ Res* 36: 153–161, 1975.
5. **Bianchi G, Fox U, Di Francesco GF, Giovanetti AM, Pagetti D.** Blood pressure changes produced by kidney cross-transplantation between spon-

Downloaded from ajprenal.physiology.org on April 27, 2009

taneously hypertensive rats and normotensive rats. *Clin Sci Mol Med* 47: 435–448, 1974.

6. **Bostanjoglo M, Reeves WB, Reilly RF, Velazquez H, Robertson N, Litwack G, Morsing P, Dorup J, Bachmann S, Ellison DH, Bostanjoglo M.** 11Beta-hydroxysteroid dehydrogenase, mineralocorticoid receptor, and thiazide-sensitive Na-Cl cotransporter expression by distal tubules. *J Am Soc Nephrol* 9: 1347–1358, 1998.
7. **Burry RW.** Specificity controls for immunocytochemical methods. *J Histochem Cytochem* 48: 163–166, 2000.
8. **Calo L, Davis PA, Semplicini A.** Control of vascular tone in the syndromes of Bartter and Gitelman. *Crit Rev Clin Lab Sci* 37: 503–522, 2000.
9. **Capasso G, Rizzo M, Evangelista C, Ferrari P, Geelen G, Lang F, Bianchi G.** Altered expression of renal apical plasma membrane Na^+ transporters in the early phase of genetic hypertension. *Am J Physiol Renal Physiol* 288: F1173–F1182, 2005.
10. **Crowley SD, Gurley SB, Herrera MJ, Ruiz P, Griffiths R, Kumar AP, Kim HS, Smithies O, Le TH, Coffman TM.** Angiotensin II causes hypertension and cardiac hypertrophy through its receptors in the kidney. *Proc Natl Acad Sci USA* 103: 17985–17990, 2006.
11. **Duc C, Farman N, Canessa CM, Bonvalet JP, Rossier BC.** Cell-specific expression of epithelial sodium channel alpha, beta, and gamma subunits in aldosterone-responsive epithelia from the rat: localization by in situ hybridization and immunocytochemistry. *J Cell Biol* 127: 1907–1921, 1994.
12. **Ecelbarger CA, Kim GH, Terris J, Masilamani S, Mitchell C, Reyes I, Verbalis JG, Knepper MA.** Vasopressin-mediated regulation of epithelial sodium channel abundance in rat kidney. *Am J Physiol Renal Physiol* 279: F46–F53, 2000.
13. **Efendiev R, Krmar RT, Ogimoto G, Zwiller J, Tripodi G, Katz AI, Bianchi G, Pedemonte CH, Bertorello AM.** Hypertension-linked mutation in the adducin alpha-subunit leads to higher AP2-mu2 phosphorylation and impaired Na^+,K^+-ATPase trafficking in response to GPCR signals and intracellular sodium. *Circ Res* 95: 1100–1108, 2004.
14. **Fanestil DD.** Steroid regulation of thiazide-sensitive transport. *Semin Nephrol* 12: 18–23, 1992.
15. **Greger R, Oberleithner H, Schlatter E, Cassola AC, Weidtke C.** Chloride activity in cells of isolated perfused cortical thick ascending limbs of rabbit kidney. *Pflügers Arch* 399: 29–34, 1983.
16. **Hager H, Kwon TH, Vinnikova AK, Masilamani S, Brooks HL, Frokiaer J, Knepper MA, Nielsen S.** Immunocytochemical and immunoelectron microscopic localization of alpha-, beta-, and gamma-ENaC in rat kidney. *Am J Physiol Renal Physiol* 280: F1093–F1106, 2001.
17. **Hanozet GM, Parenti P, Salvati P.** Presence of a potential-sensitive Na^+ transport across renal brush-border membrane vesicles from rats of the Milan hypertensive strain. *Biochim Biophys Acta* 819: 179–186, 1985.
18. **Hierholzer K, Wiederholt M, Stolte H.** The impairment of sodium resorption in the proximal and distal convolution of adrenalectomized rats. *Pflügers Arch* 291: 43–62, 1966.
19. **Hughes CA, Bennett V.** Adducin: a physical model with implications for function in assembly of spectrin-actin complexes. *J Biol Chem* 270: 18990–18996, 1995.
21. **Jeck N, Waldegger S, Lampert A, Boehmer C, Waldegger P, Lang PA, Wissinger B, Friedrich B, Risler T, Moehle R, Lang UE, Zill P, Bondy B, Schaefeler E, santo-Polus S, Seyberth H, Schwab M, Lang F.** Activating mutation of the renal epithelial chloride channel ClC-Kb predisposing to hypertension. *Hypertension* 43: 1175–1181, 2004.
22. **Jentsch TJ.** Chloride transport in the kidney: lessons from human disease and knockout mice. *J Am Soc Nephrol* 16: 1549–1561, 2005.
23. **Kaplan MR, Plotkin MD, Lee WS, Xu ZC, Lytton J, Hebert SC.** Apical localization of the Na-K-Cl cotransporter, rBSC1, on rat thick ascending limbs. *Kidney Int* 49: 40–47, 1996.
24. **Kim GH, Masilamani S, Turner R, Mitchell C, Wade JB, Knepper MA.** The thiazide-sensitive Na-Cl cotransporter is an aldosterone-induced protein. *Proc Natl Acad Sci USA* 95: 14552–14557, 1998.
25. **Kim GH, Masilamani S, Turner R, Mitchell C, Wade JB, Knepper MA.** The thiazide-sensitive Na-Cl cotransporter is an aldosterone-induced protein. *Proc Natl Acad Sci USA* 95: 14552–14557, 1998.
26. **Loffing J, Kaissling B.** Sodium and calcium transport pathways along the mammalian distal nephron: from rabbit to human. *Am J Physiol Renal Physiol* 284: F628–F643, 2003.
27. **Loffing J, Vallon V, Loffing-Cueni D, Aregger F, Richter K, Pietri L, Bloch-Faure M, Hoenderop JG, Shull GE, Meneton P, Kaissling B.** Altered renal distal tubule structure and renal Na(+) and Ca(2+) handling in a mouse model for Gitelman's syndrome. *J Am Soc Nephrol* 15: 2276–2288, 2004.
28. **Mansfield TA, Simon DB, Farfel Z, Bia M, Tucci JR, Lebel M, Gutkin M, Vialettes B, Christofilis MA, Kauppinen-Makelin R, Mayan H, Risch N, Lifton RP.** Multilocus linkage of familial hyperkalaemia and hypertension, pseudohypoaldosteronism type II, to chromosomes 1q31-42 and 17p11-q21. *Nat Genet* 16: 202–205, 1997.
29. **Mantero F, Nussdorfer GG, Robba C, Opocher G, Ferrari P, Bianchi G.** Evidence for mineralocorticoid hyperactivity in the Milan hypertensive strain of rats. *J Hypertens Suppl* 2: 150–153, 1983.
30. **Masilamani S, Kim GH, Mitchell C, Wade JB, Knepper MA.** Aldosterone-mediated regulation of ENaC alpha, beta, and gamma subunit proteins in rat kidney. *J Clin Invest* 104: R19–R23, 1999.
31. **Melzi ML, Syren ML, Assael BM, Sereni F, Aperia A.** Increased renal tubular Na-K-ATPase activity in Milan hypertensive rats in the prehypertensive period. *Pediatr Nephrol* 5: 700–703, 1991.
32. **Meyer G, Garavaglia ML, Bazzini C, Botta G.** An anion channel in guinea pig gallbladder epithelial cells is highly permeable to HCO_3^-. *Biochem Biophys Res Commun* 276: 312–320, 2000.
33. **Nissant A, Lourdel S, Baillet S, Paulais M, Marvao P, Teulon J, Imbert-Teboul M.** Heterogeneous distribution of chloride channels along the distal convoluted tubule probed by single-cell RT-PCR and patch clamp. *Am J Physiol Renal Physiol* 287: F1233–F1243, 2004.
34. **Palmer LG, Frindt G.** Cl^- channels of the distal nephron. *Am J Physiol Renal Physiol* 291: F1157–F1168, 2006.
35. **Quentin F, Chambrey R, Trinh-Trung-Tan MM, Fysekidis M, Cambillau M, Paillard M, Aronson PS, Eladari D.** The Cl^-/HCO_3^- exchanger pendrin in the rat kidney is regulated in response to chronic alterations in chloride balance. *Am J Physiol Renal Physiol* 287: F1179–F1188, 2004.
36. **Schafer JA, Watkins ML, Li L, Herter P, Haxelmans S, Schlatter E.** A simplified method for isolation of large numbers of defined nephron segments. *Am J Physiol Renal Physiol* 273: F650–F657, 1997.
37. **Scheinman SJ, Guay-Woodford LM, Thakker RV, Warnock DG.** Genetic disorders of renal electrolyte transport. *N Engl J Med* 340: 1177–1187, 1999.
38. **Sciarrone MT, Stella P, Barlassina C, Manunta P, Lanzani C, Bianchi G, Cusi D.** ACE and alpha-adducin polymorphism as markers of individual response to diuretic therapy. *Hypertension* 41: 398–403, 2003.
39. **Shimkets RA, Warnock DG, Bositis CM, Nelson-Williams C, Hansson JH, Schambelan M, Gill JR Jr, Ulick S, Milora RV, Findling JW, et al.** Liddle's syndrome: heritable human hypertension caused by mutations in the beta subunit of the epithelial sodium channel. *Cell* 79: 407–414, 1994.
40. **Simon DB, Bindra RS, Mansfield TA, Nelson-Williams C, Mendonca E, Stone R, Schurman S, Nayir A, Alpay H, Bakkaloglu A, Rodriguez-Soriano J, Morales JM, Sanjad SA, Taylor CM, Pilz D, Brem A, Trachtman H, Griswold W, Richard GA, John E, Lifton RP.** Mutations in the chloride channel gene, CLCNKB, cause Bartter's syndrome type III. *Nat Genet* 17: 171–178, 1997.
41. **Stanton BA.** Regulation by adrenal corticosteroids of sodium and potassium transport in loop of Henle and distal tubule of rat kidney. *J Clin Invest* 78: 1612–1620, 1986.
42. **Tripodi G, Valtorta F, Torielli L, Chieregatti E, Salardi S, Trusolino L, Menegon A, Ferrari P, Marchisio PC, Bianchi G.** Hypertension-associated point mutations in the adducin alpha and beta subunits affect actin cytoskeleton and ion transport. *J Clin Invest* 97: 2815–2822, 1996.
43. **Vandewalle A, Cluzeaud F, Bens M, Kieferle S, Steinmeyer K, Jentsch TJ.** Localization and induction by dehydration of ClC-K chloride channels in the rat kidney. *Am J Physiol Renal Physiol* 272: F678–F688, 1997.
44. **Velazquez H, Bartiss A, Bernstein P, Ellison DH.** Adrenal steroids stimulate thiazide-sensitive NaCl transport by rat renal distal tubules. *Am J Physiol Renal Fluid Electrolyte Physiol* 270: F211–F219, 1996.
45. **Wagner CA.** The emerging role of pendrin in renal chloride reabsorption. *Am J Physiol Renal Physiol* 292: F912–F913, 2007.
46. **Waldegger S, Jeck N, Barth P, Peters M, Vitzthum H, Wolf K, Kurtz A, Konrad M, Seyberth HW.** Barttin increases surface expression and changes current properties of ClC-K channels. *Pflügers Arch* 444: 411–418, 2002.
47. **Wang XY, Masilamani S, Nielsen J, Kwon TH, Brooks HL, Nielsen S, Knepper MA.** The renal thiazide-sensitive Na-Cl cotransporter as mediator of the aldosterone-escape phenomenon. *J Clin Invest* 108: 215–222, 2001.

Downloaded from ajprenal.physiology.org on April 27, 2009